(De)constructing the Ryanodine Receptor: Modeling Ion Permeation and Selectivity of the Calcium Release Channel

Dirk Gillespie*

Department of Molecular Biophysics and Physiology, Rush University Medical Center, Chicago, Illinois 60612

Le Xu, Ying Wang, and Gerhard Meissner

Department of Biochemistry and Biophysics, University of North Carolina, Chapel Hill, North Carolina 27599-7260

Received: May 11, 2005; In Final Form: June 22, 2005

Biological ion channels are proteins that passively conduct ions across membranes that are otherwise impermeable to ions. Here, we present a model of ion permeation and selectivity through a single, open ryanodine receptor (RyR) ion channel. Combining recent mutation data with electrodiffusion of finite-sized ions, the model reproduces the current/voltage curves of cardiac RyR (RyR2) in KCl, LiCl, NaCl, RbCl, CsCl, $CaCl_2$, $MgCl_2$, and their mixtures over large concentrations and applied voltage ranges. It also reproduces the reduced K^+ conductances and Ca^{2+} selectivity of two skeletal muscle RyR (RyR1) mutants (D4899N and E4900Q). The model suggests that the selectivity filter of RyR contains the negatively charged residue D4899 that dominates the permeation and selectivity properties and gives RyR a DDDD locus similar to the EEEE locus of the L-type calcium channel. In contrast to previously applied barrier models, the current model describes RyR as a multi-ion channel with approximately three monovalent cations in the selectivity filter at all times. Reasons for the contradicting occupancy predictions are discussed. In addition, the model predicted an anomalous mole fraction effect for Na^+/Cs^+ mixtures, which was later verified by experiment. Combining these results, the binding selectivity of RyR appears to be driven by the same charge/space competition mechanism of other highly charged channels.

Introduction

Biological ion channels conduct ions down their chemical potential gradients across cellular membranes. By opening and closing (gating) their pores in response to stimuli, groups of ion channels can initiate and propagate action potentials in neurons and release Ca^{2+} that initiates muscle contraction. In both heart and skeletal muscle, it is the ryanodine receptor (RyR) channels that release Ca^{2+} from intracellular stores in the sarcoplasmic reticulum.

As individual channels, these homotetrameric channels have been shown to be cation-selective and to have extremely large conductances for both mono- and divalent cations. Using single-channel recordings, the permeation, selectivity, and gating properties of RyR have been extensively studied[1−8] and reviewed.[9−11] Sequence comparison[12] suggested that the RyR channels have a pore architecture similar to that identified by X-ray crystallography in the bacterial KcsA potassium channel.[13] Ion permeation through RyR has been modeled, both with barrier models[14] and with Poisson−Nernst−Planck (PNP) theory.[15−17] In this paper, we present another model of RyR, one that has only recently become possible because of new mutations of RyR[8,18] and better models of electrolyte currents.[19,20]

Recent advances in the theory of ion channel selectivity have shown that highly charged channels such as the L-type calcium and neuronal (voltage-gated) sodium channels select ions by attracting cations into the channel with their high protein charge density. Ions compete for space in the confined geometry of the selectivity filter, and the selected ions are those that best neutralize (screen) the protein charges in the least amount of space.[19,21−28] Modeling this charge/space competition requires modeling ions of finite size rather than just the point-particles used in regular PNP. The Poisson−Nernst−Planck/density functional theory (PNP/DFT) model we use here is a recent generalization of PNP that describes the electrodiffusion of hard-sphere ions down their chemical potential gradients.[19,20]

Space/charge competition also requires some knowledge of the channel, especially the narrow selectivity filter where both diffusion is limited and any charged groups are at their highest concentration. In the L-type calcium and neuronal sodium channels previously studied, the approximate size of the selectivity filter is known, and some charged groups in the selectivity filter (the EEEE and DEKA loci, respectively) have been experimentally determined. For RyR, only the approximate size of the filter is known ($\sim$1 nm length and $\geq$0.35 nm in radius; reviewed by Williams et al.[9,10]).

In this paper, we use recent mutation data[8,18] to describe the selectivity filter as containing the negative residue Asp^{4899} and the lumenal atrium as containing another negative residue, Glu^{4900}. Along with some charges of unknown source in the cytosolic atrium, we use only this information about the channel to reproduce the data of RyR over a wide range of mono- and divalent ion species (including mixtures), concentrations, and applied voltages. The general closeness of the model and experimental results indicates that it is D4899 (and to a lesser

* To whom correspondence should be addressed. E-mail: dirk_gillespie@rush.edu.

10.1021/jp052471j CCC: $30.25
Published on Web 00/00/0000 PAGE EST: 12.9

extent E4900) that makes the permeation and selectivity properties of RyR.

This model is different from previous models because it describes the data by constructing RyR from experimental information about the channel structure. Both the barrier[14] and the PNP[15−17] models optimized parameters to data-fit the current/voltage curves but used no information about the channel itself apart from the selectivity filter size. Moreover, the new model accurately computes the excess chemical potentials (activities) of ions, whereas the PNP models only data-fit them.[16,17]

Here, we do not fit the data using many current/voltage points as inputs. Rather, we seek to construct the important features of RyR with D4899N and E4900Q mutant data. The input parameters such as diffusion coefficients are determined with one data point for each of the ion species to predict the data. The model predicted an anomalous mole fraction effect for Na^+/Cs^+ mixtures that was later verified by experiment. The new model is also robust, reproducing the data of the D4899N and E4900Q mutants without readjusting parameters, something not possible for the other models. We cannot make predictions about mutations outside the selectivity filter like the reduction of K^+ conductance of G4894A.[8,29]

Recently, Welch et al.[30] developed a model of the putative pore region of RyR based on the known crystal structure of the KcsA channel. No permeation or selectivity studies have been performed with this model, however, to see how well this model reproduces the experimental data. They did, however, identify several amino acids that in their simulations interact strongly with permeating ions. One of these is the equivalent of E4900, but they did not identify the equivalent of D4899.

Methods and Theory: Constructing RyR

To model ion permeation through an open RyR, both a model of ion transport and a model of the RyR channel are needed.

Model of Ion Transport. Here, we model ions as charged, hard spheres and water as uncharged, hard spheres. For this ion model, a computationally inexpensive model to compute ion flux has been developed by Gillespie et al.[19] In brief, the model describes the motion of ions and water through a channel by diffusion and drift along the electrostatic mean field. The general three-dimensional problem is reduced to one dimension along the axis of the channel by assuming cylindrical symmetry and averaging the concentration profiles over equi-chemical potential surfaces with area $A(x)$ (where this surface intersects the axis of the channel at x).[31] The flux J_i of ion species i is described by the constitutive relationship

$$-J_i = \frac{1}{kT} D_i(x) A(x) \rho_i(x) \frac{d\mu_i}{dx} \qquad (1)$$

where $D_i(x)$ is the local diffusion coefficient, $\rho_i(x)$ is the local concentration, and $\mu_i(x)$ is the local chemical potential. The chemical potential of the charged, hard spheres is computed using density functional theory (DFT) of fluids as described by Gillespie et al.[19,20] In the case of uncharged point particles, this theory reduces to Fick's law of diffusion, and in the case of charged point particles, it reduces to PNP theory. This approach has recently also been used in other systems where the results have compared well to more accurate simulations.[32,33]

Model of the Channel. Because there is no high-resolution structure of the RyR permeation pathway, we used a reduced model of the channel as a central cylindrical selectivity filter connected to the baths on each side by a conical atrium (Figure 1). The selectivity filter was made 1 nm in length and 0.4 nm in radius, in accordance with current estimates.[6,9] The atria were each made 2 nm long with their walls at a 45° angle to the channel axis. Each bath was made 1 μm long. Concentration and potential boundary conditions were applied at the edges of the baths, far from the channel. These parameters were never changed except when studying the effect of reducing the channel radius half an angstrom to 0.35 nm.

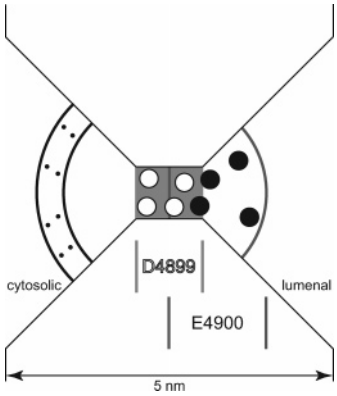

Figure 1. Geometry of the model channel. The oxygens of D4899 (hollow spheres) are confined to the center selectivity filter (gray region). The oxygens of E4900 (solid spheres) are confined from the middle of the selectivity filter into the right (lumenal or trans) atrium (dark gray lines). Because of limited space in the cross-section shown, only four of the eight oxygens are shown for both D4899 and E4900, while much of the space in the selectivity filter is taken up by particles; in the three-dimensional model (shown here in cross-section), there is enough space for the oxygens and the mobile ions. The cytosolic atrium charge is modeled as fixed point charges evenly distributed throughout the volume indicated in the left (cytosolic or cis) atrium with dots. The confining boundaries are curved because of the one-dimensional approximation to the full three-dimensional equations.[31] The sharp corners at the atrium/membrane and atrium/filter junctions are rounded in the calculation. The lumenal side is defined as ground.

With detailed modeling of all RyR amino acid residues impossible, we chose instead to construct RyR from the bottom up by including amino acid residues determined by experiments to be important for permeation. By including only a very small number of these residues while at the same time reproducing the data of the entire channel, we aim to show that it is these residues that are responsible for most of the permeation and selectivity properties of RyR.

To choose the important residues, we focused on charged residues that significantly reduced channel conductance when mutated. In other channels such as the L-type calcium channel and the neuronal sodium channel, such charged residues tend to drive permeation and selectivity, as shown both by experiment[34−38] and by simulation.[19,21−27,38,39] By this criterion, we chose to include Asp^{4899} and Glu^{4900} in the model because mutations that replaced their residues with similar ones with no charge significantly reduced conductance. Furthermore, these D4899N and E4900Q mutants retained wild-type ryanodine binding and still conducted Ca^{2+}, indicating minimal changes in channel structure.[8,18] While the G4894A mutant also significantly reduced conductance,[8,29] we included only charged residues. Currently, it is not clear how the G4894A mutation affects the channel.

Both aspartate and glutamate have a charged carboxyl group, the only part of the residue that we modeled. The carboxyl groups were fully charged in all calculations, and protonation was not considered. Because it has been successful in the past when applied to calcium and sodium channels, we modeled each COO^- as two uncoupled, half-charged oxygen ($O^{1/2-}$) molecules

confined to a region of the channel but subject to the same forces as all the other ions.[19,21−27,38] The average location of the oxygens within the confinement region is an output of the calculation and changes when the contents of the channel changes (i.e., when the voltage or bath concentrations are changed).

With four aspartates (one from each of the four RyR subunits), the eight oxygens representing D4899 were confined to the central selectivity filter. To reduce the number of input parameters, this was never changed. We chose to put D4899 into the smallest part of the channel where diffusion is the most limited because the mutant D4899N (i.e., turning off the charge of the carboxyl group) reduces RyR conductance to 10−20% of normal, the largest change in conductance of the two mutants D4899N and E4900Q.[8,18]

The eight oxygens from the four glutamates E4900 (one from each of the four subunits that make up RyR) were also confined to a region. It was not clear a priori where they should be confined except that it should be near D4899 (because the oxygens represent E4900). Therefore, the starting and ending points of confinement for E4900 were included in the list of input parameters that needed to be determined.

To start, no other amino acids were included in the analysis, but in the course of the modeling, it was determined that more charge was needed in the cytosolic atrium to reproduce the current/voltage curve at low K^+ concentrations.

Determining Input Parameters. The input parameters for the model fall into two categories: particle and channel.

General Parameters. For the mobile particles (ions and water), the diameter, charge, and diffusion coefficient profile (throughout the system) must be known for each species. For the confined oxygens, the diffusion coefficient is not necessary because they do not contribute to the measured particle current.[19] As we have done before,[19,21−28,38] we chose crystal diameters for all particles as determined by Shannon and Prewitt.[40] The charge of each particle is, of course, straightforward. When modeling the mutants D4899N and E4900Q, the charge on the oxygens was set to zero, and no other adjustments were made.

The diffusion coefficient for each species is only known in the baths[41,42] and must be determined for the inside of the channel. To reduce the number of inputs, the diffusion coefficient profile for each species was divided into three regions: the selectivity filter (with D4899), the region with E4900, and everywhere else (the cytosolic and lumenal baths and the atria not occupied by channel oxygens). One constant diffusion coefficient was determined for each region and then Gauss-filtered with a 0.2 nm wide peak. The only purpose of filtering the profile was to produce a smooth profile without jumps.

With the channel dimensions (radius, length, and atrium geometry) assumed given and set for all calculations, the only remaining channel parameter is the size and location of the confining region of the E4900 oxygens.

Channel and K^+ Parameters. Given a set of starting and ending coordinates for the E4900 oxygens, the two undetermined diffusion coefficient parameters were determined for K^+ by simultaneously fitting two data points (the current at +100 mV for native RyR and the current at +20 mV for E4900Q, both in symmetric 250 mM KCl solutions). The E4900 confinement range was determined by comparing the current/voltage curve of each guess of the confinement range to the experimental D4899N data. The best fit was determined by eye and corresponded to a starting position in the center of the selectivity filter and extending into the lumenal atrium. In total, the E4900 oxygens occupied a volume 3.75 times larger than the selectivity filter (Figure 1). In this way, the confining regions of D4899and E4900 overlap on the lumenal side of the selectivity filter; having the two regions not overlap produced poor agreement with the D4899N data.

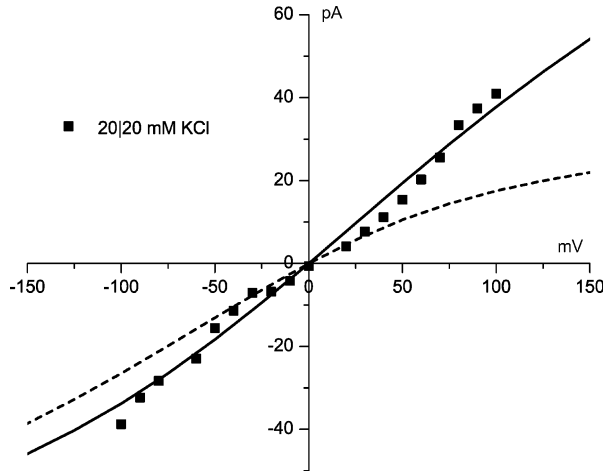

Figure 2. Current/voltage curve in 20 mM symmetric KCl (■). The model is with (solid line) and without (dashed line) the cytosolic atrial charge.

Additional Charge in the Cytosolic Atrium. In the process of evaluating the channel and K^+ parameters, all the data were reproduced qualitatively well except for the current/voltage curve for 20 mM symmetric KCl; the model predicted current rectification instead of a linear current/voltage relationship. To reproduce this 20 mM KCl data, eight negative charges were placed into the cytosolic atrium. Because the exact amino acid residues represented by these charges were unknown and because they were located in a very wide part of the channel, the charges were modeled as immobile (fixed) point charges evenly distributed throughout a volume 5.7 times the filter volume (Figure 1). Because the model is one-dimensional, these (and all) charges were spread over a volume and could not be placed on the atrium walls.

The channel parameters (e.g., location of the E4900 oxygens) were unchanged, and the K^+ diffusion coefficient profile was refit as described previously. The diffusion coefficient for K^+ was computed to be 6.84×10^{-11} m^2/s in the selectivity filter and 3.28×10^{-10} m^2/s in the E4900 region (the part outside the selectivity filter). With the extra cytosolic atrial charge, all the data fit quantitatively well, including the 20 mM symmetric KCl case (Figure 2, solid line). In contrast to the results of this paper, Tu et al.[7] found current rectification at low monovalent concentrations. This may be because of their use of sarcoplasmic reticulum vesicles that contain the negatively charged calsequestrin complex; here we used purified RyR.

To understand the impact of the cytosolic atrial charges, we can mutate (in the computer) the model channel to remove these charges. When they are not present, the current at low KCl concentration rectifies (Figure 2, dashed line). Furthermore, the loss of the cytosolic atrial charges reduces the conductance approximately 10−15% in 250 mM symmetric KCl solutions (to 680 pS). All model results shown here and all further parameter calculations include this cytosolic atrial charge.

Diffusion Coefficients. With all the channel and K^+ parameters established and unchanging, the diffusion coefficients for each of the other cations were determined from just *one* data point. For the monovalent cations, this point was the current at +100 mV in symmetric 250 mM solutions. For the divalent

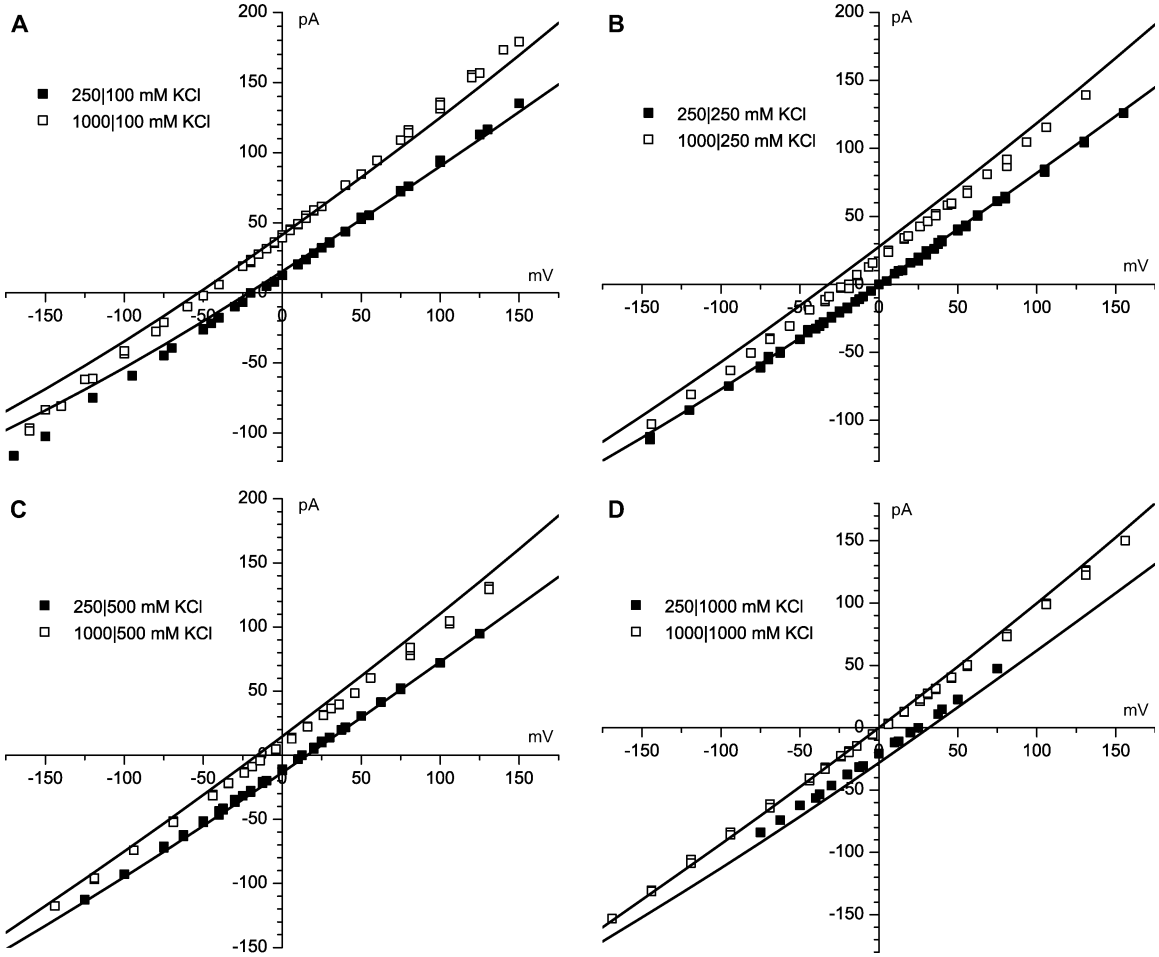

Figure 3. Current/voltage curves in KCl with 250 mM (■) or 1000 mM (□) cytosolic bath concentrations and (A) 100 mM, (B) 250 mM, (C) 500 mM, and (D) 1000 mM lumenal bath concentrations. In this and all figures, the solid lines are the results of the model.

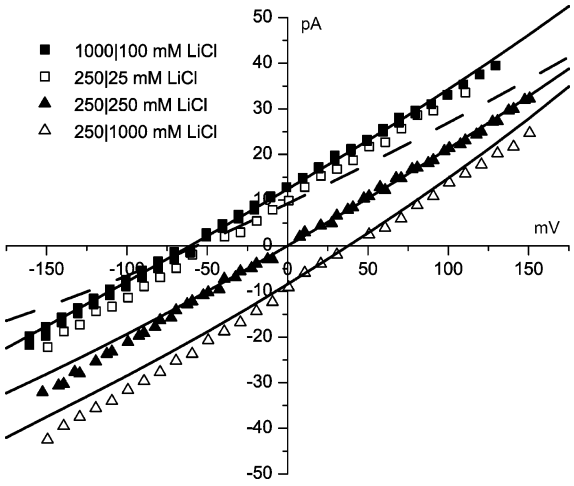

Figure 4. Current/voltage curves in LiCl. The dashed line is the model result for 250 mM cytosolic and 25 mM lumenal bath concentrations (□).

ions, this point was the current at −100 mV in symmetric 250 mM KCl solutions with 10 mM $CaCl_2$ or $MgCl_2$ in the lumenal bath.

To reduce the number of inputs and so only one data point was necessary, it was assumed that the diffusion coefficient in the E4900 region for all ions was 4.8 times that of the selectivity filter, just as for K^+. With this process, except for the one data point used to determine the diffusion coefficient profile, all the model outputs for non-K^+ cations (Li^+, Na^+, Rb^+, Cs^+, Ca^{2+}, Mg^{2+}, and their mixtures) are direct tests of the channel model. The diffusion coefficients in the selectivity filter were calculated to be (in m^2/s) Li^+, 1.29×10^{-11}; Na^+, 3.92×10^{-11}; Rb^+, 5.57×10^{-11}; Cs^+, 4.11×10^{-11}; Ca^{2+}, 2.75×10^{-12}; and Mg^{2+} 2.94×10^{-12}. After the diffusion coefficients were determined, they were never changed, even in ion mixtures.

Inside the selectivity filter, water and Cl^- were given diffusion coefficients 1% of their bath values. No attempt was made to optimize these values. Setting either the water or Cl^- diffusion coefficients inside the channel to bulk values only changed the current/voltage curves by approximately 1%. Water is excluded from the channel because it is uncharged and therefore easy to displace from the high-density selectivity filter. Cl^- is almost completely excluded from the cation-selective selectivity filter because of its negative charge and large size.

For the cations, the selectivity filter diffusion coefficients are 1−4% of bulk for monovalents and 0.4% of bulk for divalents. This reduction is due to two contributions: the confining geometry of the narrow pore and the high density of the fluid in the selectivity filter. Specifically, molecular dynamics (MD) simulations of water molecules or of a single ion in channels show a reduction of diffusion coefficients by a factor of 5−10.[43,44] Also, ion diffusion coefficients are reduced in a highly concentrated electrolyte solution like that inside the selectivity filter (Figures 10−12). In MD simulations of 14.4 molal aqueous KF, Laudernet et al.[45] found that the bulk diffusion coefficient of K^+ was reduced by an order of magnitude from the infinitely dilute bulk value we use in the baths. Combining these two contributions gives the 1% of bulk that we found from the data

fitting. For divalent ions, the ion pairing Laudernet et al.[45] found will be much more pronounced and reduce these diffusion coefficients even more.

In summary, the adjustable parameters were (1) the selectivity filter radius, (2) the starting and ending locations of the E4900 confinement zone, (3) the amount of cystolic atrial charge, (4) two diffusion coefficients for K^+, and (5) one diffusion coefficient for all other cations.

With a given selectivity filter radius, the E4900 confinement zone, cytosolic charge, and K^+ diffusion coefficients were determined simultaneously by fitting two data points and comparing the predicted and experimental current/voltage curves for D4899N in symmetric 250 mM KCl and for native RyR in symmetric 20 mM KCl. Once these geometrical and K^+ parameters were determined, they were never changed, even when ion concentrations changed, the baths contained ion mixtures, or RyR mutations were studied. The diffusion coefficients of the other cations were then determined by fitting exactly one data point. Once these diffusion coefficients were calculated, they were never changed, even when ion concentrations changed, the baths contained ion mixtures, or RyR mutations were studied. The data used to estimate these parameters were a very small fraction of the available data; therefore, almost all the calculated current/voltage points were predictions of the model.

Other parameters that we could have changed, but chose not to, were (1) the length of the selectivity filter, (2) the shape of the channel geometry, and (3) the location of the cystolic atrial charge. These were fixed at the start of the analysis and never changed. A reasonable estimate for the selectivity filter length was available, and no information currently exists about the permeation pathway geometry or the location of cytosolic charged amino acids at the necessary resolution.

Robustness of the Parameters. The parameters that we have established for RyR are not absolute but are meant as general guidelines. For example, we assumed the general shape of the diffusion coefficient function and then determined parameters within that constraint.

The diffusion coefficients are robust in the sense that changing them changes the computed current. The same cannot be said of some of the channel parameters. For example, changing the location of the E4900 oxygens and the cytosolic atrium charges by a few angstroms has very little effect on the computed current. This is consistent with the general principle that we have applied here: knowledge of the exact location of the channel amino acids is in many cases unimportant; rather, it is the general location that matters. For instance, we only confine the D4899 and E4900 oxygens to compartments in which they are free to arrange themselves.

Experiments also show that this is the case. For example, the neuronal sodium channel can be mutated into a calcium channel by changing the DEKA locus into a DEEE locus, similar to the EEEE locus found in the L-type calcium channel.[34] These channels are homologous but not so closely related to imply that the geometry of the DEEE locus is exactly the same as the EEEE locus. In general, having a channel whose properties are not tied to the exact location of certain amino acids makes the channel more robust and resistant to misfolding and mutations.

What Is and Is Not in the RyR Model? Our model of RyR contains the ideas that in previous studies we have found dominate the physics of ion permeation and selectivity: (1) the movement of ions down their chemical potential gradients (eq 1) with self-consistently computed electrostatics,[46] (2) excluded volume (ions of finite size that cannot overlap),[19,21−28,38] (3)

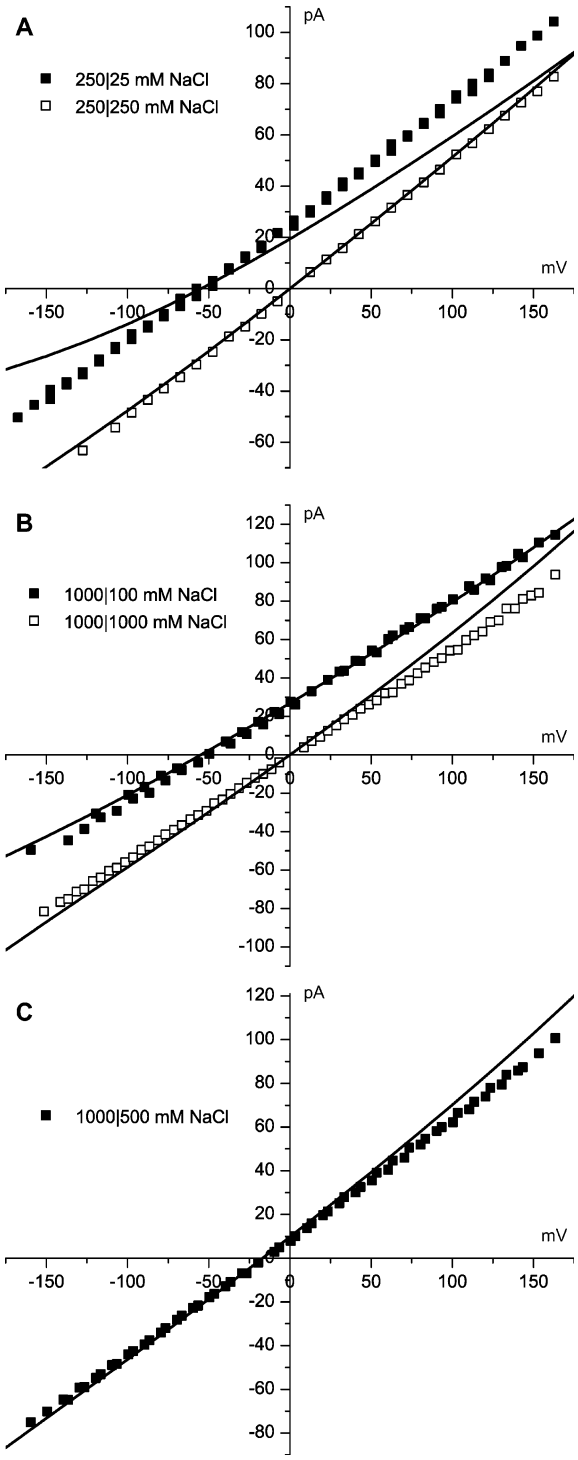

Figure 5. Current/voltage curves in NaCl.

selected protein amino acid residues that dominate the permeation and selectivity process,[19,21−27,38] and (4) the movement of these dominant residues (when they are in the permeation pathway) due Coulombic forces and the excluded volume of ions.

This model does not include other aspects found in more sophisticated models: (1) polarization of the channel protein and bilayer membrane (here the dielectric coefficient is 78.4 throughout the system), (2) cohesive forces between particles, in particular hydration of ions (we only include excluded-volume and electrostatic interactions with water as an uncharged sphere), and (3) the exact location of all (or even most) amino acid residues of the channel protein. In the case of RyR, the physics

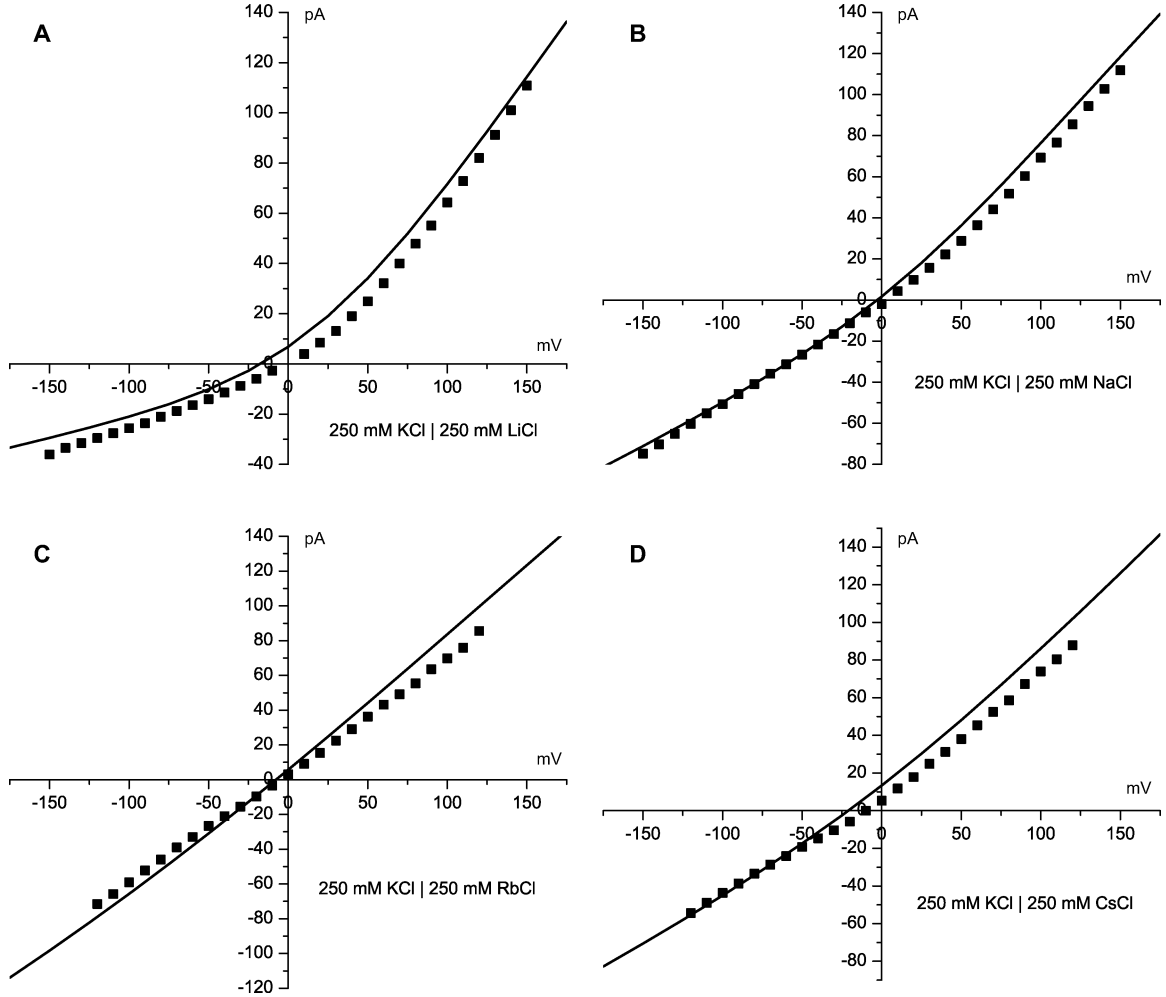

Figure 6. Current/voltage curves in bi-ionic conditions. In the cytosolic bath is 250 mM KCl, and in the lumenal bath is 250 mM (A) LiCl, (B) NaCl, (C) RbCl, and (D) CsCl.

we have included is sufficient to explain its permeation and selectivity properties.

Experimental Data. Single channel measurements were performed as previously described using Mueller−Rudin-type planar lipid bilayers containing a 5:3:2 mixture of bovine brain phosphatidylethanolamine, phosphatidylserine, and phosphatidylcholine (25 mg of total phospholipid/mL of *n*-decane).[18] Proteoliposomes containing the purified RyRs were added to the cis (sarcoplasmic reticulum cytosolic) chamber of the bilayer apparatus and fused with the lipid bilayer. Single channel currents were measured with the indicated buffer solutions on both sides of the lipid bilayer and 2−20 μM Ca^{2+} and 1 mM or no ATP in the cis chamber of the bilayer apparatus. The trans (sarcoplasmic reticulum lumenal) side of the bilayer was defined as ground. Electrical signals were filtered at 2 kHz, digitized at 10 kHz, and analyzed as described.[18]

The current/voltage relations for RyR2 have been previously reported by Chen et al.[15−17] The data for the mutant D4899N were reported by Gao et al.[8], and the data for E4900Q were reported by Wang et al.[18] All data are from the RyR2 (cardiac muscle) isoform except the mutation data, which are from the RyR1 (skeletal muscle) isoform. The two isoforms have very similar permeation and selectivity properties.[11] Because the mutations were made with RyR1, we use the sequence numbering of RyR1 throughout this paper;[47] the corresponding RyR2 mutations are D4830N and E4831Q.[48]

Results

Monovalent Cations. First, we compare the experimentally determined current/voltage curves and the model results for KCl (Figure 3 and Supporting Information Figure 1), LiCl (Figure 4), NaCl (Figure 5), RbCl (Supporting Information Figure 2), and CsCl (Supporting Information Figure 3) solutions. D4899N and E4900Q in KCl solutions are shown in Figure 9.

Bi-Ionic Conditions. Figure 6 compares the experimentally determined current/voltage curves and the model results for bi-ionic conditions with 250 mM solutions of KCl|LiCl, KCl|NaCl, KCl|RbCl, and KCl|CsCl. Supporting Information Figure 4 shows more bi-ionic KCl|LiCl current/voltage curves.

Mole Fraction Experiments. Next, we consider mole fraction experiments with monovalent cations where the total cation concentration is 250 mM. Figure 7A shows the mole fraction conductance for the Li^+/K^+ mixture. As has been reported before, the channel conductance decreases nonlinearly (but monotonically) as the mole fraction of Li^+ increases,[5,16] indicating a small-ion preference in binding selectivity.[49] Other monotonically changing mole fraction experiments have also been reported (reviewed by Williams et al.[9]). For the ion mixtures tested, RyR does not exhibit an anomalous mole fraction effect (AMFE) where the conductance reaches a minimum or a maximum.

Because of the fast computation time of the model, we were able to test all possible Li^+, Na^+, K^+, Rb^+, and Cs^+ combinations for an AMFE. As shown in Figure 7B, we found that the

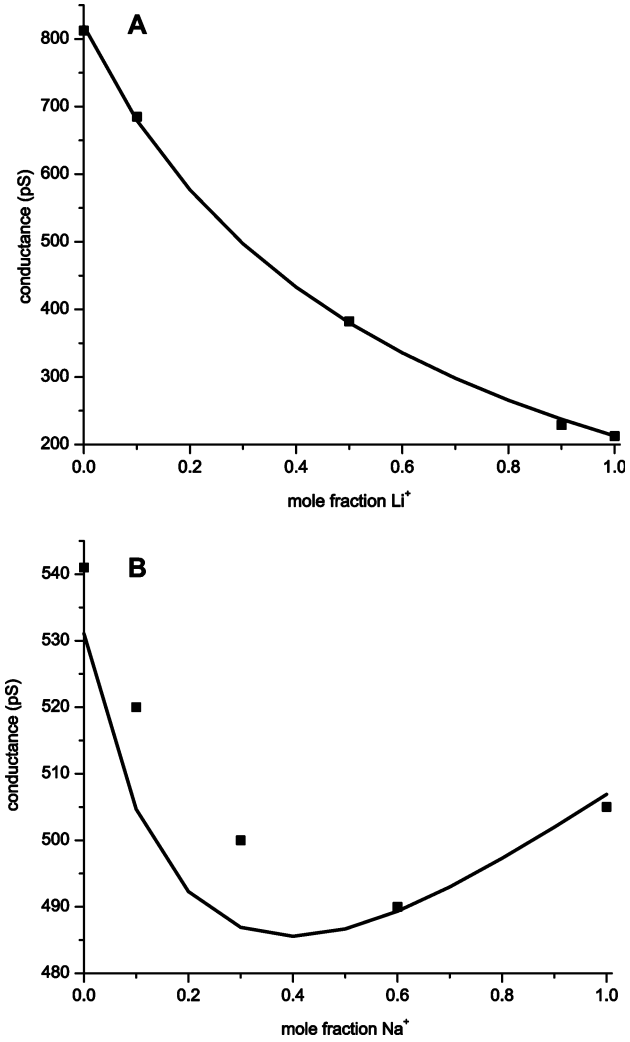

Figure 7. Mole fraction experiments at 250 mM total cation concentration in symmetric solutions. (A) LiCl and KCl mixtures. (B) NaCl and CsCl mixtures.

Na^+/Cs^+ mixture does exhibit an AMFE. This was a pure prediction of the model; the experiment was done after the calculation.

Divalent Cations. Figure 8 compares the experimentally determined current/voltage curves to the model results for divalent cations: Ca^{2+} with KCl (Figure 8A), NaCl (Figure 8B), and CsCl (Figure 8C) solutions and Mg^{2+} with a KCl solution (Figure 8D).

Mutations. Figure 9 compares the experimentally determined current/voltage curves to the model results for the mutants D4899N and D4900Q.

Discussion: Deconstructing RyR

Using a one-dimensional electrodiffusion model of ions with finite size, we reproduced the data of RyR and two mutants. In general, the fit of the data was very good—but not perfect. There is some general misfit: reversal potentials in alkali metal chloride solutions are slightly off; for all alkali metal chloride solutions, the conductance for the 250|25 mM case is too small; and the computed bi-ionic current/voltage curves are shifted to the left. The errors in the alkali metal chloride reversal potentials are due to the inability to perfectly compute individual activity coefficients, a general problem of physical chemistry theories. Quantitatively, the error in the conductance is only on the order of 10% (see Figure 16B).

It is, however, the overall closeness of the model predictions that should be observed. The model is a minimalist model in an oversimplified channel geometry; it contains only electrodiffusion of finite-sized ions and two explicitly modeled channel amino acids (and one area of charge in the cytosolic atrium of an unresolved origin). The overall quantitative correctness of the model suggests that electrodiffusion of ions through a selectivity filter containing D4899 and E4900 dominates permeation and selectivity in RyR and that other important physical phenomena (i.e., hydration of ions and polarization of the channel protein and bilayer membrane)—as well as all the other amino acids along the permeation pathway—are of secondary importance for permeation and selectivity.

Calculated Concentration Profiles. *Native versus Mutated RyR.* Figures 10 and 11 show the model's predictions of the average concentrations along the pore axis: K^+ (Figure 10A), D4899 and E4900 oxygens (Figure 11A), and water (Figure 11B). Figure 11C shows the mean electrostatic potential profile. In native RyR (solid lines), there is a high concentration of K^+ in the selectivity filter that has been attracted by the high concentration of negative D4899 oxygens. The selectivity filter is very electronegative, and the electrostatic potential is very nonlinear across the channel (Figure 11C); the channel does not follow the common assumption of charge-neutrality everywhere, which would result in a linear voltage drop across the channel.

In the E4900Q mutant (Figure 10A, dashed line), the K^+ concentration profile is nearly identical to that of the native channel (solid line)—except that the concentration is much reduced in the lumenal atrium, similar to the electrostatic potential (Figure 11C). Even though there is a large amount of K^+ in the selectivity filter itself, the conductance of E4900Q is much less than of the native channel (compare Figures 3B and 9A) because the mutant's lumenal atrium K^+ concentration is reduced.

Dramatic changes in the profiles occur for the D4899N mutant (dotted line). Because the protein charge concentration that attracts K^+ into the selectivity filter has been removed, there is more than a 20-fold reduction in the K^+ concentration in the filter, causing the dramatic reduction from normal conductance (compare Figures 3B and 9A).

Effect of Ca^{2+}. The model predicts that K^+ in the pore is replaced by Ca^{2+} when Ca^{2+} is added to the lumenal bath (Supporting Information Figure 5). The current is blocked not only because there is less K^+ in the channel but also because the Ca^{2+} in the selectivity filter moves slower than the K^+; the diffusion coefficient of Ca^{2+} is 4% of the diffusion coefficient of K^+ (Figure 10B). When 10 mM Ca^{2+} is added to the lumenal bathing solution, the pore of the D4899N mutant (Figure 12, dotted lines) contains relatively little K^+ or Ca^{2+}. E4900Q, on the other hand, contains a higher concentration of K^+ than the native channel (Figure 12, dashed lines) but a lower concentration of Ca^{2+}; the loss of protein charge (Figure 11A) in E4900Q has lowered the Ca^{2+} affinity as compared to native RyR, and K^+ displaces the Ca^{2+} from the selectivity filter to neutralize D4899.

RyR Has the Signature of a Classic Calcium Channel. With our model, almost all permeation and selectivity properties are accounted for by D4899 and E4900. We decided to explicitly model these two amino acids because the neutralization of their charges (the mutants D4899N and E4900Q) produced large changes in conductance apparently without changing the RyR structure.[8,18] D4899N produced the largest change, reducing conductance to 10−20% of normal;[8] therefore, we chose to place

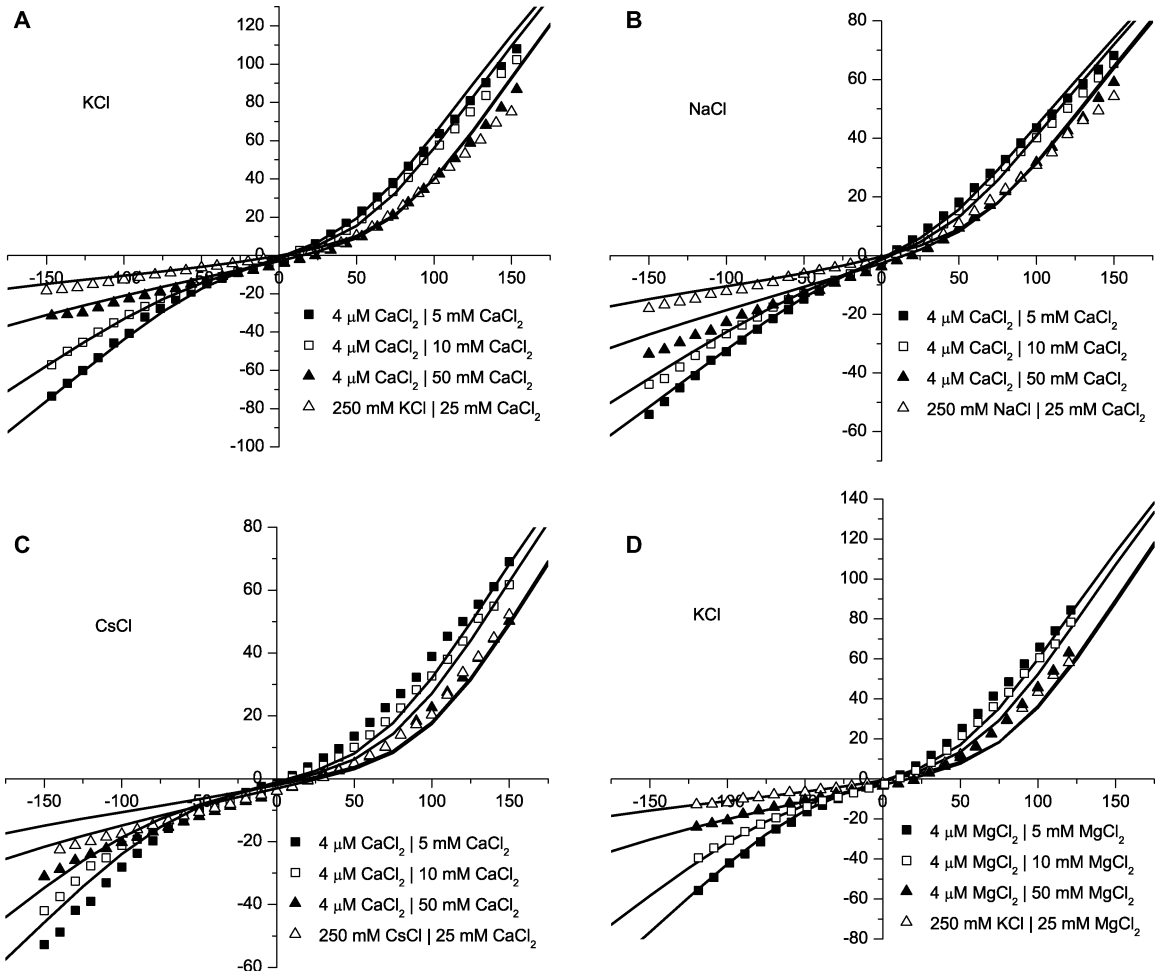

Figure 8. Current/voltage curves with divalent and monovalent cations. (A) KCl and $CaCl_2$, (B) NaCl and $CaCl_2$, (C) CsCl and $CaCl_2$, and (D) KCl and $MgCl_2$. In both baths is 250 mM monovant-Cl, and in the lumenal bath is 5 mM (■), 10 mM (□), and 50 mM (▲) divalent-Cl_2, or the baths contain 250 mM cytosolic monovant-Cl and 25 mM lumenal divalent-Cl_2 (Δ).

this residue in the smallest part of the channel (the selectivity filter described in Methods and Theory).

Because RyR is a homotetramer, the resulting DDDD structure in a very small volume is a motif nearly identical to the EEEE locus of the L-type calcium channel.[34−37] (Aspartate and glutamate are identical except that the side chain of the glutamate is longer.) Therefore, from the point of view of this model, RyR has the signature of a classic calcium channel, and it is the DDDD locus that creates most of the permeation and selectivity properties of RyR. This motif has also been seen in other Ca^{2+}-conducting channels such as the vanilloid receptor[50] and the glutamate receptor.[51]

While E4900 contributes to these properties (Figures 9−12), in the model, D4899 is in the diffusion-limited part of the channel and is at a much higher density than E4900 (D4899 is in a smaller volume). Therefore, D4899 is responsible for the majority of the flux properties (by limiting diffusion) and ion binding (by having high charge density). This is also seen experimentally; D4899N reduces the conductance to 10−20% of normal, while E4900Q only reduces conductance to 60% of normal.

Other theoretical studies of calcium-selective channels also support this view; model channels with four highly confined carboxyl groups (like those of aspartate or glutamate residues) have the same millimolar Ca^{2+} affinity as RyR, as measured by the block of monovalent current shown in Figure 8A−C. (Ca^{2+} block is studied by Gillespie et al.[19] and Miedema et al.;[38] Ca^{2+} binding is studied by Boda et al.[23−25,2]) Attraction and coordination of Ca^{2+} by carboxyl groups is also common in other Ca^{2+}-binding molecules, like in the EF-hand motif of many Ca^{2+}-binding proteins (reviewed by Nelson and Chazin[52]) and in Ca^{2+} chelators such as EGTA.

While it is true that the L-type calcium channel has micromolar Ca^{2+} affinity, this is believed to involve weak dielectric polarizability in the selectivity filter region.[21,22,53] Similarly, the local environment near an EF-hand motif greatly affects Ca^{2+} affinity.[52] Therefore, it is possible for both RyR and L-type calcium channels to have the DDDD/EEEE locus, but also very different Ca^{2+} affinities, if the local environment of the loci are different (i.e., the proteins have different polarizability).

RyR Is a Multi-Ion Channel. Our electrodiffusion model shows that RyR is a multiply occupied channel with approximately three K^+ cations in the selectivity filter alone and many more in the entire channel (Figure 13A). When $CaCl_2$ is added on the lumenal side, K^+ is displaced by Ca^{2+}, with the occupancy of Ca^{2+} approaching two (Figure 13B). Barrier models, on the hand, indicate that RyR is singly occupied.[5,14]

The evidence usually cited to conclude single occupancy (reviewed by Williams et al.[9,10]) includes (1) saturation of conductance with increasing ion activity, (2) concentration-independent bi-ionic reversal potentials if bath ion activity ratios are constant, and (3) the lack of an AMFE. The relationships between these phenomena and channel occupancy are, however, model-dependent. Because the two models use very different physics to describe ion permeation,[54] they come to opposite conclusions on these relationships. These relationships were

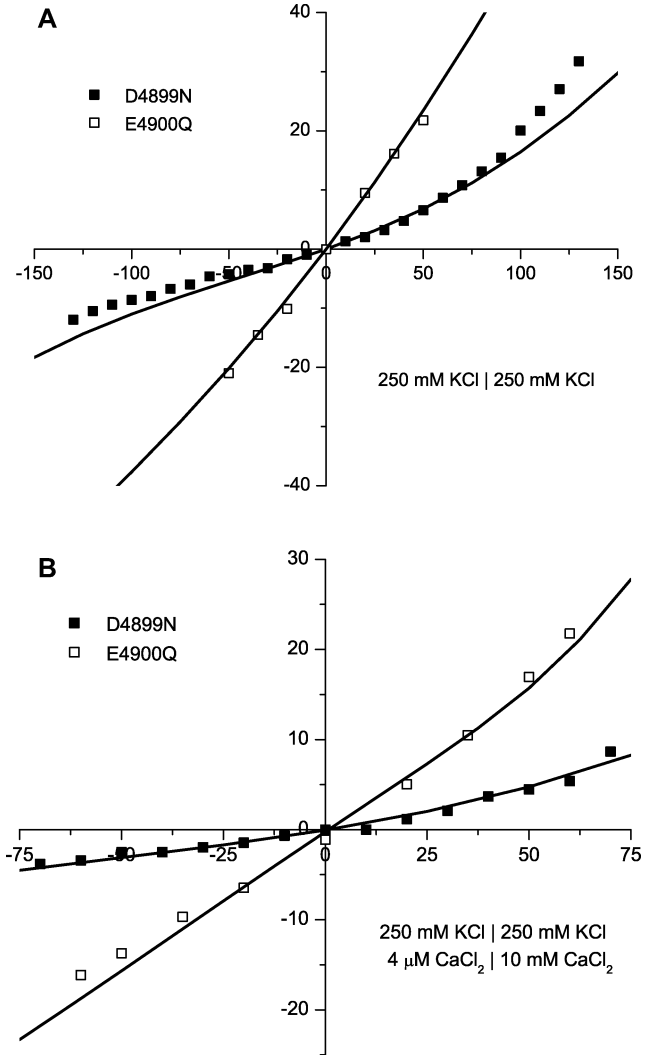

Figure 9. (A) Current/voltage curves of the D4899N (■) and E4900Q (□) mutants in 250 mM symmetric KCl. (B) Current/voltage curves of the D4899N (■) and E4900Q (□) mutants in 250 mM symmetric KCl and 10 mM lumenal $CaCl_2$.

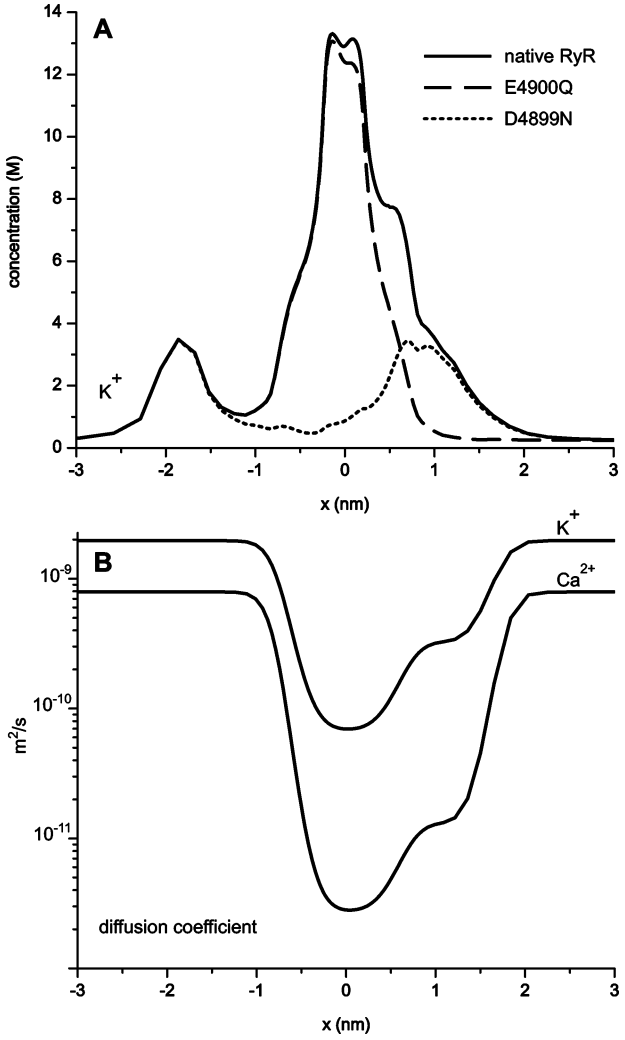

Figure 10. (A) Calculated concentration profiles along the permeation axis of the channel for K^+ in the absence of Ca^{2+}. In both baths is 250 mM KCl, and no voltage is applied. The selectivity filter is located between ±0.5 nm. The profiles are for the native RyR channel (solid lines), the E4900Q mutant (dashed lines), and the D4899N mutant (dotted lines). (B) The diffusion coefficient profiles of K^+ and Ca^{2+} along the permeation axis. These were the same for the mutants.

derived using barrier models and are not true in an electrodiffusion model like the one used here. The model used here exhibits conductance saturation while having multiple ions in the channel. Moreover, Gillespie and Eisenberg[49] showed that the PNP model used by Chen et al.[15−17] exhibits both conductance saturation and bi-ionic reversal potential property regardless of occupancy. Nonner et al.[55] have also shown that it is possible for channels containing less than one ion (on average) to exhibit an AMFE.

The most often cited evidence for single-ion occupancy is the lack of an AMFE. To understand more about the AMFE from the electrodiffusion point of view, consider the occupancy of the selectivity filter in Li^+/K^+ and Na^+/Cs^+ mixtures (Figure 14). In both cases, the total occupancy (the sum of the two cations) is approximately the same and approximately constant over the entire range of mole fractions. Moreover, between the two calculations, the occupancy of the small ions (Li^+ and Na^+) is nearly the same, as is the occupancy of the large ions (K^+ and Cs^+). One experiment has an AMFE and the other does not because the occupancy of the channel is dominated by electrostatics with the screening of the charged residues.

In general, the AMFE arises from the same physics that causes the mole fraction conductance to deviate from linearity: a highly attracted ion (in this case the smaller cation) that moves through the channel more slowly (has a lower diffusion coefficient) than the other ion. When a small amount of the more attracted ion is added, its presence depresses the channel current. Because the K^+ current is so much larger than the Li^+ current, the channel current cannot be depressed enough to cause a minimum. For the other case, however, Na^+ and Cs^+ have approximately the same conductance (510 and 540 pS, respectively) so that addition of Na^+ can depress the current enough to cause a minimum (that is, an AMFE). For a detailed discussion, see the discussion by Nonner et al.[55]

To reconcile the different predictions of the barrier and electrodiffusion models, we must examine the models themselves. Electrodiffusion as modeled here includes physics that is present in real solutions (movement of ions down chemical gradients, self-consistent electrostatics, and excluded volume of ions); it does not include all physics, but what it does contain is also present in real fluids.[56−61]

This is not true for barrier models, which describe ion permeation as ions hopping over energy barriers. The Eyring (gas-phase) barrier models used to describe RyR[9,14] use a prefactor of incorrect mathematical form that is approximately 4 orders of magnitude too large.[15,31,54,62,63] Moreover, barrier

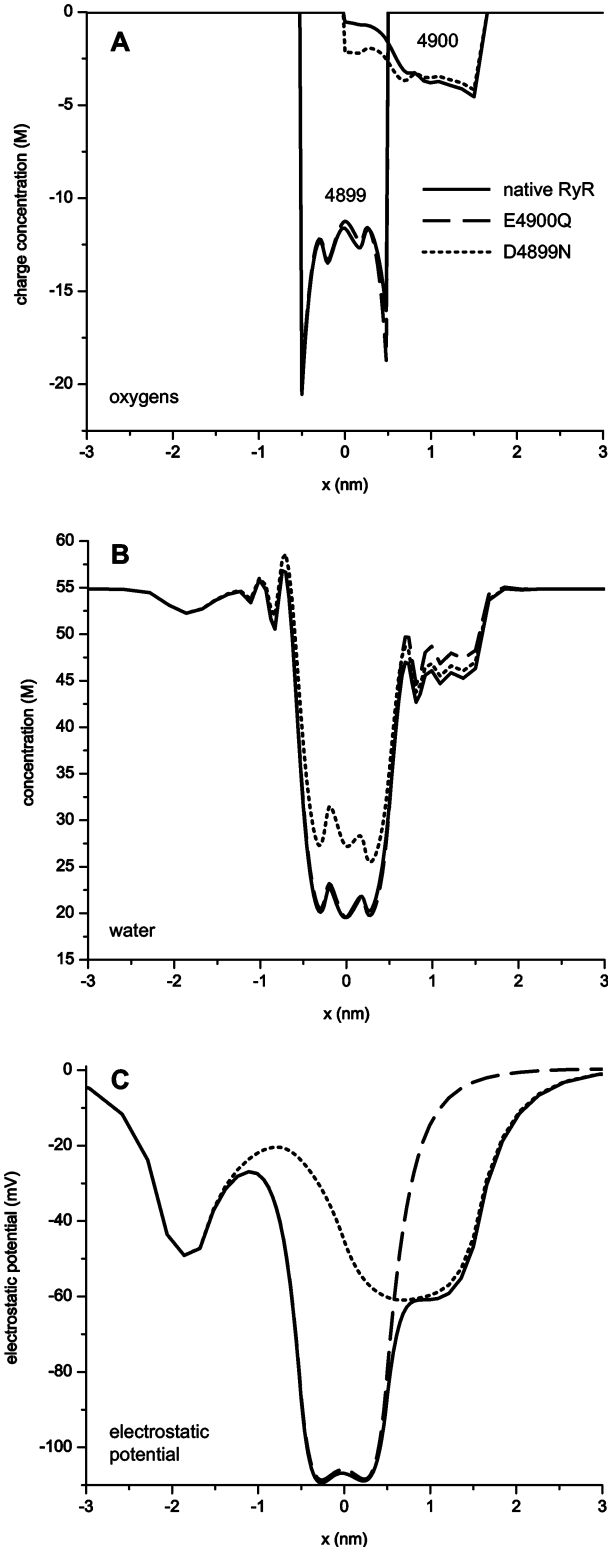

Figure 11. Calculated profiles along the permeation axis for native and mutant RyR. The bath concentrations are the same as in Figure 10. (A) The charge concentration (not particle concentration) of the D4899 and E4900 oxygens. In the D4899N mutant, the charge comes only from E4900 (dotted line) and in the E4900Q mutant only from D4899 (dashed line). When oxygens are charged, the plotted concentration is −1/2 the particle concentation because the oxygens have a −1/2 charge. (B) The water concentration. (C) The electrostatic potential.

models assume ion trajectories (rather than compute them) with an electric field that is inconsistent with Maxwell's laws of electrodynamics.

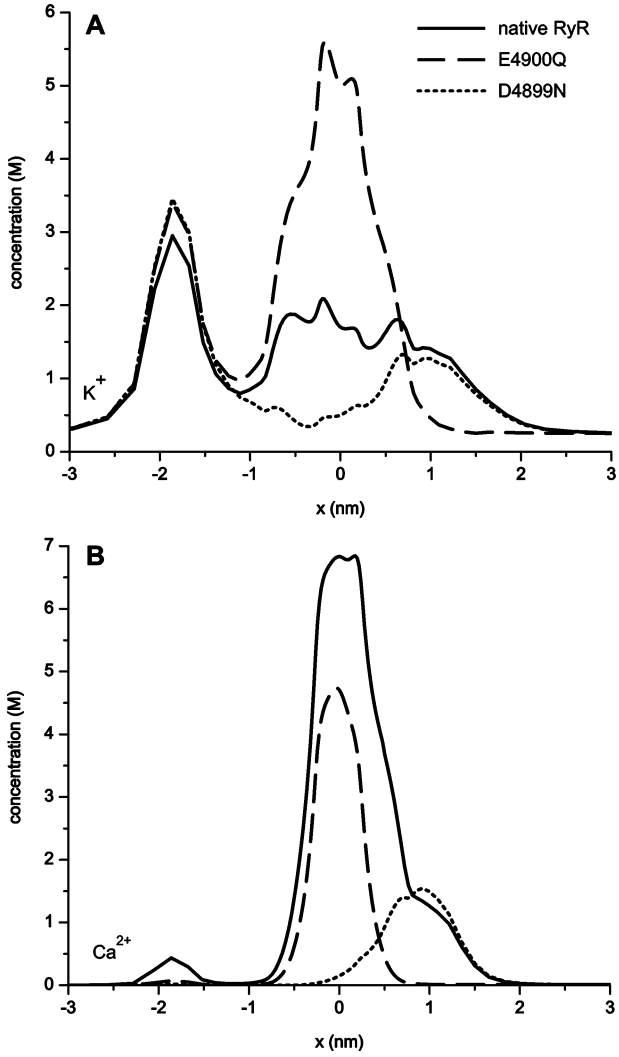

Figure 12. Calculated concentration profiles of native and mutant RyR along the permeation axis of the channel for (A) K^+ and (B) Ca^{2+}. The profiles are for the native RyR channel (solid lines), the E4900Q mutant (dashed lines), and the D4899N mutant (dotted lines). In both baths is 250 mM KCl, and in addition, the lumenal bath contains 10 mM $CaCl_2$. No voltage is applied.

Selectivity: Charge/Space Competition. In our model, the two amino acids responsible for almost all of the selectivity properties are D4899 and E4900. What has not been addressed yet is the physical mechanism used by these amino acids to produce these selectivity properties. Because, according to our model, the selectivity filter of RyR is very similar to a classic calcium channel, the answer for binding selectivity is already known: charge/space competition (CSC). (Gillespie and Eisenberg[49] have a discussion of the different kinds of selectivity measured by different selectivity experiments.)

As described previously, the selectivity filter of RyR contains highly concentrated charges at approximately 13 M. The CSC (also called crowded charge) principle describes the selectivity in such a highly attractive channel as a competition between the need to neutralize (screen) the charges of the protein (the DDDD locus) and the limited space in the selectivity filter. Ideally, the most energetically favorable situation is to have charge neutrality in the selectivity filter, but because the ions have a finite size and cannot overlap, when two cation species are in the baths and in direct competition to neutralize the protein charges, it is the smallest cations that best fit into the filter to screen the carboxyl groups. This has been verified by many different calculations using several different models.[19,21−28,38]

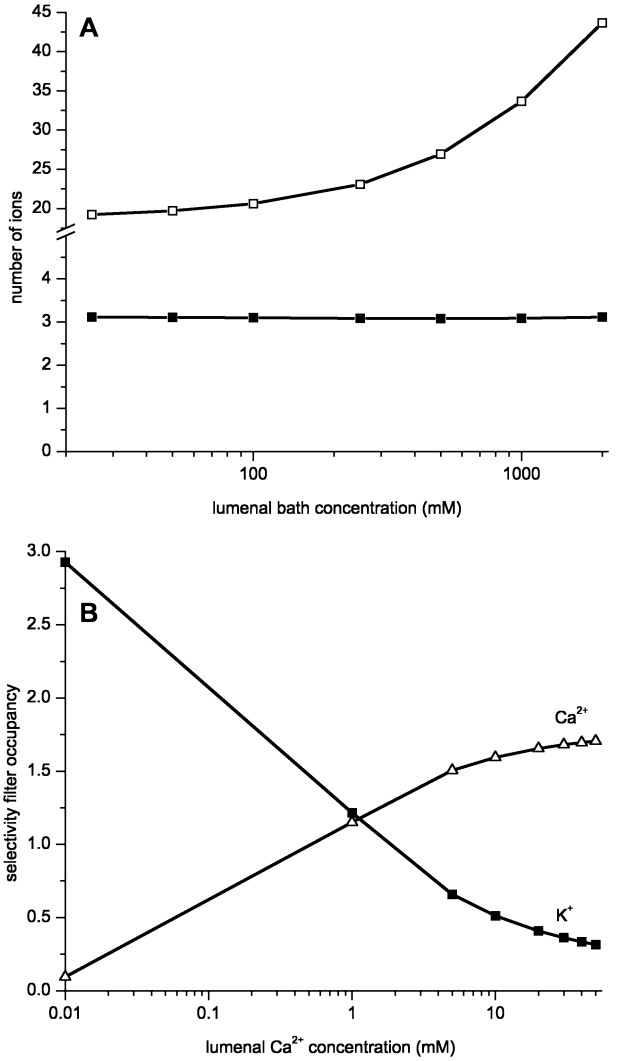

Figure 13. (A) Number of K^+ ions in the selectivity filter (■) and in the entire channel (the filter and the two atria) (□) for 250|*x* mM KCl solutions with no applied potential. (B) The number of K^+ (■) and Ca^{2+} (Δ) ions in the selectivity filter for symmetric 250 mM KCl solutions and *x* mM lumenal $CaCl_2$ with no applied potential.

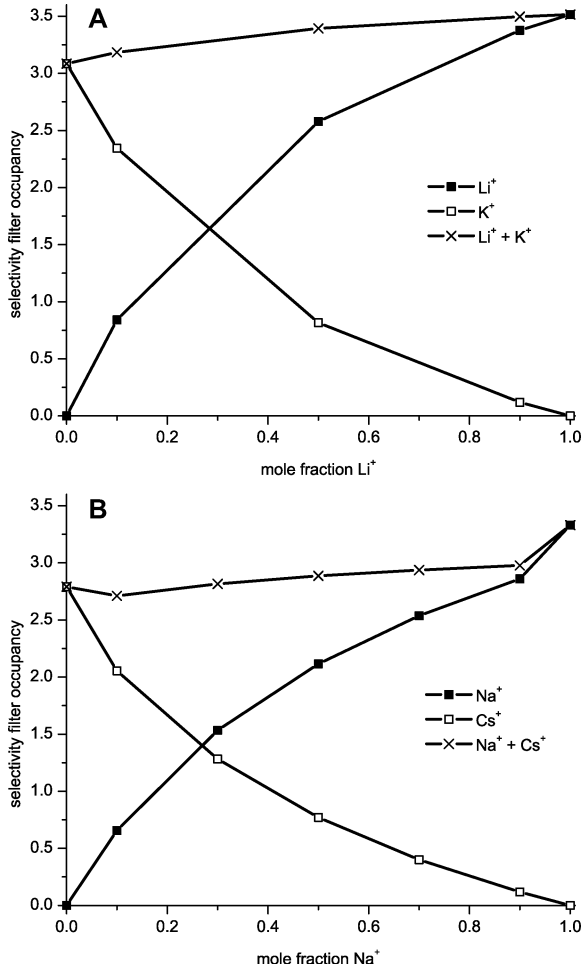

Figure 14. Number of each cation in the selectivity filter in mole fraction experiments. The total number of cations (×) is also shown. (A) Li^+ (■) and K^+ (□). (B) Na^+ (■) and Cs^+ (□).

In these calculations, as in this paper, the ions were assumed to be dehydrated, and the energy to strip off the hydration shell was neglected.

For RyR, the CSC mechanism can be demonstrated by reducing the channel radius from 0.4 to 0.35 nm. This smaller value is the estimated minimum radius of RyR (reviewed by Williams et al.[9,10]) and has been used to model RyR.[15−17] After refitting the ion parameters as described previously using the smaller radius, all the alkali metal chloride solution current/voltage curves are reproduced with the same accuracy as for the 0.4 nm radius channel. This is not a surprise; even with the more narrow channel, the cations can still get into the selectivity filter to approximately the same extent.[49] As predicted by CSC, the differences are apparent when there is a mixture of cations in the baths—that is, when ions are in direct competition. For example, with less space in the channel, the more narrow channel is more Ca^{2+}-selective, depressing the Cs^+ current more than in the wider channel (compare outward currents in Figures 15A and 8C); the smaller and more charged Ca^{2+} can more effectively screen the protein charges than the large Cs^+ in the more narrow channel. Also, in the Na^+/Cs^+ mole fraction experiment, the calculated AMFE is more pronounced with the narrower channel because this channel has a higher affinity for small ions (in this case Na^+) (Figure 15B). It is because the model results for the 0.35 nm radius channel did not fit as well as for the 0.4 nm radius channel that we chose to use the wider channel.

Conclusion

We have shown that the permeation and selectivity properties of RyR and two of its mutants are captured by an electrodiffusion model of hard-sphere ions. The model does not attempt to interpret other mutation data.[8,18,29] The idea of charge/space competition implicit in the model explains both the small-ion binding selectivity and the high conductance of RyR by predicting a high-occupancy selectivity filter. The model is also predictive of current/voltage data. The source of the cytosolic structural charge remains to be investigated.

Appendix: Computing Bath Activities

In our model, the flux J_i of each particle species *i* is given by[19]

$$J_i = \frac{\exp(\mu_i(L)/kT) - \exp(\mu_i(R)/kT)}{\int \exp(\mu_i(x)/kT)[\rho_i(x)D_i(x)A(x)]^{-1}\mathrm{d}x} \qquad (2)$$

where $\mu_i(L)$ and $\mu_i(R)$ are the individual chemical potentials of species *i* in the left (cytosolic) and right (lumenal) baths, respectively. Because the model channel is (almost) perfectly cation-selective, in pure XCl solutions, the reversal potential is

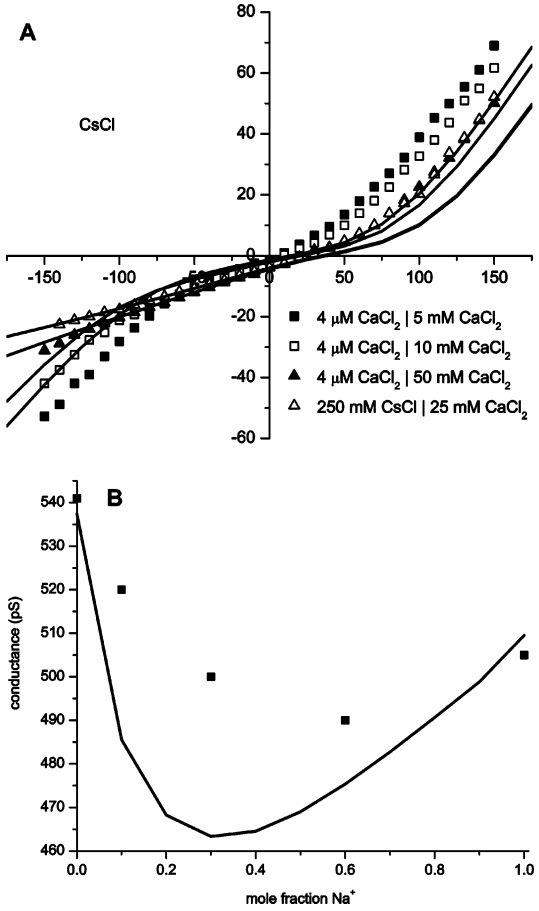

Figure 15. Increased small-ion selectivity when changing the channel radius from 0.4 to 0.35 nm. (A) Excessive block of (outward) Cs^+ current by Ca^{2+}. Compare to the block of outward Cs^+ current calculated with the wider channel in Figure 8C. The symbols are the same as those in Figure 8. (B) The Na^+/Cs^+ mole fraction experiment calculated for the narrower channel. The computed conductance minimum is more pronounced than with the wider channel, indicating that the 0.35 nm channel is more small-ion selective.

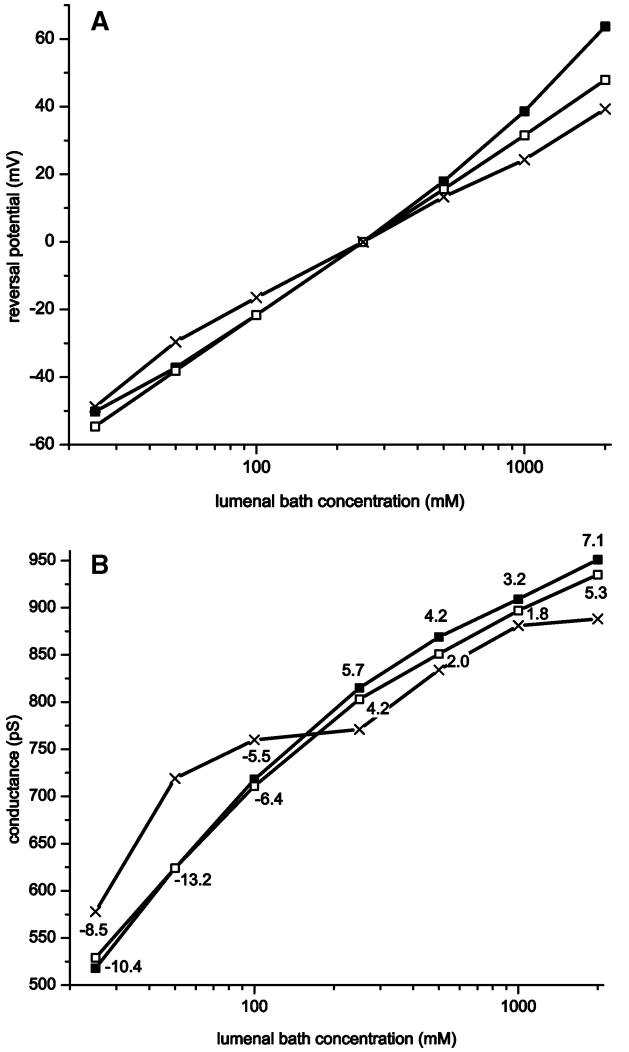

Figure 16. (A) Reversal potentials for 250|*x* mM KCl solutions: calculated without the Simonin correction (■); calculated with the Simonin correction (□); and experimental (×). (B) Slope conductances at reversal potential for 250|*x* mM KCl solutions: calculated without the Simonin correction (■); calculated with the Simonin correction (□); and experimental (×). The numbers are the relative error of the calculations as compared to the experimental value. Both the reversal potentials and the conductances were calculated by fitting a line through the data points approximately 30 mV on each side of the reversal potential.

given by the relation $\mu_{X+}(L) = \mu_{X+}(R)$, which gives the Nernst potential; in other words, the reversal potential is solely determined by the individual chemical potentials (activities) of the cation X^+ in the baths. Therefore, to compute the reversal potential, the model must correctly compute the individual chemical potentials of all alkali metal ions—and their mixtures in other experiments.

However, there are no perfect theories for this. Simonin et al.[64,65] have introduced a data-fit theory to compute mean activities with less than 1% error; individual activities cannot be compared to reliable experiments.[66] In their homogeneous system, Simonin et al. used concentration-dependent ion diameters and dielectric coefficients, an idea that cannot be applied to the inhomogeneous DFT calculations where ion diameters and dielectric coefficients are set at the start of the calculation. To compute accurate ion activities in the baths in the DFT, we did the following.

We took the individual Simonin activities to be the activities of the ions. To match these activities with the activities computed by the model, we adjusted the bath concentrations and bath potential in our model, the only parameters available for change. The resulting adjustment was minimal. A 250 mM KCl solution that contained 54.9 M water at 25 °C now contained 246 mM KCl and 54.9 M water. The electrostatic potential of the bath changed by 0.4 mV. These small changes reproduced the Simonin bath activities and resulted in a closer and more consistent fit of the reversal potentials as compared to not using the Simonin activities (Figure 16A).

This adjustment in concentrations to compute bath activities only affected the calculation of the reversal potential; the conductance of the model channel was unaffected. As discussed, the reversal potential of RyR was determined by the chemical potentials of the cation in the baths. The conductance, however, was determined by the channel, and this we computed correctly with or without the Simonin corrections, as shown in Figure 16B. The adjustment of concentrations is an issue of physical chemistry, not of channel biophysics.

When divalent cations were in the baths, we made no Simonin adjustment of bath concentrations because of the high affinity of RyR for divalents; small changes in divalent concentrations have disproportionately large effects.

Acknowledgment. The authors thank Tom Shannon and Eduardo Ríos for useful comments on the manuscript. D.G. also thanks Bob Eisenberg and Wolfgang Nonner for their careful

criticisms of the manuscript and for their suggestions concerning the treatment of bath ions. This work was supported by NIH Grants 067241 (D.G.) and AR18687 and HL73051 (G.M.).

Supporting Information Available: Figures showing current/voltage curves for KCl, RbCl, and CsCl solutions; bi-ionic KCl|LiCl current/voltage curves; and calculated concentration profiles of native RyR along the permeation axis of the channel for K^+ and Ca^{2+}. This material is available free of charge via the Internet at http://pubs.acs.org.

References and Notes

(1) Smith, J. S.; Coronado, R.; Meissner, G. *Nature* **1985**, *316*, 446−449.
(2) Smith, J. S.; Coronado, R.; Meissner, G. *J. Gen. Physiol.* **1986**, *88*, 573−588.
(3) Smith, J. S.; Imagawa, T.; Ma, J.; Fill, M.; Campbell, K. P.; Coronado, R. *J. Gen. Physiol.* **1988**, *92*, 1−26.
(4) Lai, F. A.; Erickson, H. P.; Rousseau, E.; Liu, Q. Y.; Meissner, G. *Nature* **1988**, *331*, 315−319.
(5) Lindsay, A. R.; Manning, S. D.; Williams, A. J. *J. Physiol. (London)* **1991**, *439*, 463−480.
(6) Tu, Q.; Velez, P.; Brodwick, M.; Fill, M. *Biophys. J.* **1994**, *67*, 2280−2285.
(7) Tu, Q.; Velez, P.; Cortes-Gutierrez, M.; Fill, M. *J. Gen. Physiol.* **1994**, *103*, 853−867.
(8) Gao, L.; Balshaw, D.; Xu, L.; Tripathy, A.; Xin, C.; Meissner, G. *Biophys. J.* **2000**, *79*, 828−840.
(9) Williams, A. J.; West, D. J.; Sitsapesan, R. *Q. Rev. Biophys.* **2001**, *34*, 61−104.
(10) Williams, A. J. *Frontiers Biosci.* **2002**, *7*, 1223−1230.
(11) Meissner, G. *Cell Calcium* **2004**, *35*, 621−628.
(12) Balshaw, D.; Gao, L.; Meissner, G. *Proc. Natl. Acad. Sci. U.S.A.* **1999**, *96*, 3345−3347.
(13) Doyle, D. A.; Morais Cabral, J.; Pfuetzner, R. A.; Kuo, A.; Gulbis, J. M.; Cohen, S. L.; Chait, B. T.; MacKinnon, R. *Science* **1998**, *280*, 69−77.
(14) Tinker, A.; Lindsay, A. R.; Williams, A. J. *J. Gen. Physiol.* **1992**, *100*, 495−517.
(15) Chen, D.; Xu, L.; Tripathy, A.; Meissner, G.; Eisenberg, B. *Biophys. J.* **1997**, *73*, 1337−1354.
(16) Chen, D. P.; Xu, L.; Tripathy, A.; Meissner, G.; Eisenberg, B. *Biophys. J.* **1999**, *76*, 1346−1366.
(17) Chen, D.; Xu, L.; Eisenberg, B.; Meissner, G. *J. Phys. Chem. B* **2003**, *107*, 9139−9145.
(18) Wang, Y.; Xu, L.; Pasek, D. A.; Gillespie, D.; Meissner, G. *Biophys. J.* **2005**, *89*, 256−265.
(19) Gillespie, D.; Nonner, W.; Eisenberg, R. S. *J. Phys.: Condens. Matter* **2002**, *14*, 12129−12145.
(20) Gillespie, D.; Nonner, W.; Eisenberg, R. S. *Phys. Rev. E* **2003**, *68*, 031503.
(21) Nonner, W.; Catacuzzeno, L.; Eisenberg, B. *Biophys. J.* **2000**, *79*, 1976−1992.
(22) Nonner, W.; Gillespie, D.; Henderson, D.; Eisenberg, B. *J. Phys. Chem. B* **2001**, *105*, 6427−6436.
(23) Boda, D.; Busath, D. D.; Henderson, D.; Sokolowski, S. *J. Phys. Chem. B* **2000**, *104*, 8903−8910.
(24) Boda, D.; Henderson, D.; Busath, D. D. *J. Phys. Chem. B* **2001**, *105*, 11574−11577.
(25) Boda, D.; Henderson, D.; Busath, D. D. *Mol. Phys.* **2002**, *100*, 2361−2368.
(26) Boda, D.; Busath, D.; Eisenberg, B.; Henderson, D.; Nonner, W. *Phys. Chem. Chem. Phys.* **2002**, *4*, 5154−5160.
(27) Boda, D.; Henderson, D. *J. Phys.: Condens. Matter* **2002**, *14*, 9485−9488.
(28) Roth, R.; Gillespie, D., in preparation.
(29) Zhao, M.; Li, P.; Li, X.; Zhang, L.; Winkfein, R. J.; Chen, S. R. W. *J. Biol. Chem.* **1999**, *274*, 25971−25974.
(30) Welch, W.; Rheault, S.; West, D. J.; Williams, A. J. *Biophys. J.* **2004**, *87*, 2335−2351.
(31) Nonner, W.; Eisenberg, B. *Biophys. J.* **1998**, *75*, 1287−1305.
(32) Marconi, U. M. B.; Tarazona, P. *J. Chem. Phys.* **1999**, *110*, 8032−8044.
(33) Penna, F.; Tarazona, P. *J. Chem. Phys.* **2003**, *119*, 1766−1776.
(34) Heinemann, S. H.; Terlau, H.; Stuhmer, W.; Imoto, K.; Numa, S. *Nature* **1992**, *356*, 441−443.
(35) Mikala, G.; Bahinski, A.; Yatani, A.; Tang, S.; Schwartz, A. *FEBS Lett.* **1993**, *335*, 265.
(36) Yang, J.; Ellinor, P. T.; Sather, W. A.; Zhang, J.-F.; Tsien, R. *Nature* **1993**, *366*, 158−161.
(37) Ellinor, P. T.; Yang, J.; Sather, W. A.; Zhang, J.-F.; Tsien, R. *Neuron* **1995**, *15*, 1121−1132.
(38) Miedema, H.; Meter-Arkema, A.; Wierenga, J.; Tang, J.; Eisenberg, B.; Nonner, W.; Hektor, H.; Gillespie, D.; Meijberg, W. *Biophys. J.* **2004**, *87*, 3137−3147.
(39) Corry, B.; Allen, T. W.; Kuyucak, S.; Chung, S.-H. *Biophys. J.* **2001**, *80*, 195−214.
(40) Shannon, R. D.; Prewitt, C. T. *Acta Crystallogr.* **1969**, *B25*, 925−946.
(41) Robinson, R. A.; Stokes, R. H. *Electrolyte Solutions*, 2nd ed.; Butterworth Scientific Publications: London, 1959.
(42) *CRC handbook of chemistry and physics*, 84th ed.; Lide, D. R., Ed.; CRC Press: Boca Raton, FL, 2003.
(43) Tieleman, D. P.; Berendsen, H. J. C. *Biophys. J.* **1998**, *74*, 2786−2801.
(44) Smith, G. R.; Sansom, M. S. P. *Biophys. J.* **1998**, *75*, 2767−2782.
(45) Laudernet, Y.; Cartailler, T.; Turq, P.; Ferrario, M. *J. Phys. Chem. B* **2003**, *107*, 2354−2361.
(46) Eisenberg, R. S. *J. Membr. Biol.* **1996**, *150*, 1−25.
(47) Takeshima, H.; Nishimura, S.; Matsumoto, T.; Ishida, H.; Kangawa, K.; Minamino, N.; Matsuo, H.; Ueda, M.; Hanaoka, M.; Hirose, T.; Numa, S. *Nature* **1989**, *339*, 439−445.
(48) Nakai, J.; Imagawa, T.; Hakamata, Y.; Shigekawa, M.; Takeshima, H.; Numa, S. *FEBS Lett.* **1990**, *271*, 169.
(49) Gillespie, D.; Eisenberg, R. S. *Eur. Biophys. J.* **2002**, *31*, 454−466.
(50) Garcia-Martinez, C.; Morenilla-Palao, C.; Planells-Cases, R.; Merino, J. M.; Ferrer-Montiel, A. *J. Biol. Chem.* **2000**, *275*, 32552−32558.
(51) Panchenko, V. A.; Glasser, C. R.; Mayer, M. L. *J. Gen. Physiol.* **2001**, *117*, 345−360.
(52) Nelson, M. R.; Chazin, W. J. *BioMetals* **1998**, *11*, 297.
(53) Boda, D.; Gillespie, D.; Nonner, W.; Henderson, D.; Eisenberg, B. *Phys. Rev. E* **2004**, *69*, 046702.
(54) Nonner, W.; Chen, D. P.; Eisenberg, B. *J. Gen. Physiol.* **1999**, *113*, 773−782.
(55) Nonner, W.; Chen, D. P.; Eisenberg, B. *Biophys. J.* **1998**, *74*, 2327−2334.
(56) Berry, S. R.; Rice, S. A.; Ross, J. *Physical Chemistry*, 2nd ed.; Oxford: New York, 2000.
(57) Fawcett, W. R. *Liquids, Solutions, and Interfaces: From Classical Macroscopic Descriptions to Modern Microscopic Details*; Oxford University Press: New York, 2004.
(58) Barthel, J.; Krienke, H.; Kunz, W. *Physical Chemistry of Electrolyte Solutions: Modern Aspects*; Springer: New York, 1998.
(59) Rowley, R. L. *Statistical Mechanics for Thermophysical Calculations*; PTR Prentice Hall: Englewood Cliffs, NJ, 1994.
(60) Henderson, D. *Fundamentals of Inhomogeneous Fluids*; Marcel Dekker: New York, 1992.
(61) Hansen, J.-P.; McDonald, I. R. *Theory of Simple Liquids*; Academic Press: New York, 1986.
(62) Hänggi, P.; Talkner, P.; Borokovec, M. *Rev. Mod. Phys.* **1990**, *62*, 251−341.
(63) Eisenberg, R. S.; Kłosek, M. M.; Schuss, Z. *J. Chem. Phys.* **1995**, *102*, 1767−1780.
(64) Simonin, J.-P.; Blum, L.; Turq, P. *J. Phys. Chem.* **1996**, *100*, 7704−7709.
(65) Simonin, J.-P. *J. Phys. Chem. B* **1997**, *101*, 4313−4320.
(66) Khoshkbarchi, M.; Vera, J. H. *AIChE J.* **1996**, *42*, 249−258.